Particlelike nature of colliding three-dimensional optical solitons

D. E. Edmundson and R. H. Enns
Department of Physics, Simon Fraser University, Burnaby, British Columbia, Canada V5A 1S6
(Received 26 August 1994)

Numerical scattering experiments in a medium characterized by a simple saturable refractive index demonstrate the particlelike behavior of three-dimensional bright optical envelope solitons ("light bullets") for the situation where the colliding bullets initially have a π-phase difference and are on the positive-slope branch of the energy curve. By varying the initial bullet velocities, bullet energy content, and the impact parameter, the nature of the repulsive interaction potential (i.e., the force law) is ascertained to be a Yukawa potential whose decay constant agrees quite well with that obtained by assuming that each light bullet "sees" only the "tail" of the other bullet. The scattering data scale correctly with velocity and one finds that the bullet energy is the natural analog of particle mass.

PACS number(s): 42.65.Pc, 42.50.Rh

I. INTRODUCTION

In 1990, Silberberg [1] suggested the possible existence of a stable three-dimensional bright optical envelope soliton which could arise in suitable bulk, dispersive, nonlinear media when an optical pulse is able to propagate without change because the longitudinal dispersive and transverse diffractive effects are both balanced by nonlinear compression. While Silberberg's paper was concerned with the production of exceptionally high electric fields as a spherical pulse collapsed in a medium possessing a Kerr-like nonlinear refractive index, in closing he noted that saturation of the Kerr nonlinearity could possibly halt this singular collapse, causing the formation of a stable "light bullet." The correctness of this conjecture has been verified by the theoretical investigations of Enns and co-workers [2–5] and Akhmediev and Soto-Crespo [6].

Because of their ongoing interest in optical bistability, Enns and Rangnekar [2] showed that bistable light bullets could exist in bulk media characterized by two saturable jumps. Rather than search for an "exotic" material with this requisite behavior, such a media could be formed [3] as an appropriate "mixture" of media with simple (single jump) saturable refractive indices. Bistable light bullets are propagating, spheroidal, bright optical envelope solitons characterized by different sizes and intensity profiles but with the same energy. At a given bullet energy, the low state is characterized by a broader profile with a low intensity center, while the corresponding high state is smaller and much more intense. Edmundson and Enns [4] numerically demonstrated the robustness of bistable light bullets against large perturbations with collision and switching simulations for two representative double saturable refractive index models.

More recently, Akhmediev and Soto-Crespo [6] have shown numerically (assuming cylindrical symmetry) that a longitudinally modulated cylindrical light beam in a simple saturable medium spontaneously forms into a train of light bullets—the optical "machine gun." Edmundson and Enns [5] then exploited the full three- (spatial) dimensional nature of the problem by breaking cylindrical symmetry and performing numerical collisions between pairs of light bullets at arbitrary impact parameters. Preliminary results were reported relevant to both single and double saturable models. Several novel effects were discovered, some of which have no one-dimensional analog. With zero initial phase difference between the bullets, the tunneling of a high state bistable soliton through a much larger low state soliton was observed. When two identical in-phase solitons were collided at low velocity and grazing incidence, the attractive force between them led to orbital capture, the light bullets eventually fusing, leaving a single rotating soliton core [7].

As in one-dimension [8], the attractive or repulsive nature of the interaction force between two solitons was observed to depend on the initial phase difference between them. Of particular interest, and the subject of this paper, is the particlelike behavior observed when the phase difference between two identical colliding solitons is π, in this case the force law being repulsive. Confining our attention to a simple saturable model of the intensity dependent refractive index (which is representative of semiconductor doped glasses and certain organics [9]), we have carried out numerical scattering experiments to determine the approximate structure of the interaction potential. To interpret the scattering data, which involves measuring the asymptotic scattering angle θ as a function of the impact parameter b, we can select the "correct" force law by comparison with the results obtain using the scattering formula (e.g., see Landau and Lifshitz, Chap. 4 [10]) of classical mechanics for a particle being elastically scattered by a central potential. Although very computationally demanding (being a three-dimensional space + time problem), this approach clearly demonstrates the particle or billiard-ball-like behavior of the colliding light bullets. Since the simple saturable refractive index model is characteristic of existing materials, this particlelike behavior should be verifiable in the laboratory.

II. THEORY

Light bullet propagation in bulk, anomalously dispersive, nonlinear media is governed (in the group velocity frame) by the three space + time generalized nonlinear Schrödinger equation (GNLSE)

$$iE_z + \frac{1}{2}(E_{xx} + E_{yy} + E_{tt}) + f(I=|E|^2)E = 0. \quad (1)$$

Here $E \propto \phi$, the complex electric field amplitude; z and x, y are proportional to the propagation (z_1) and transverse (x_1,y_1) distances, respectively; $t \propto (t_1 - z_1/v_g)$, where t_1 is the time and v_g the group velocity; and $f(I)$ is a nonlinear function proportional to the intensity (I) dependent part of the refractive index. For the Kerr nonlinearity, $f(I) = I$ and the NLSE of Ref. [1] is regained. Stable light bullets do not exist for this case. Applying Silberberg's conjecture, here we restrict ourselves to the simple saturable model $f(I) = I/(1 + aI)$ with a being a reciprocal measure of the saturation intensity. The nonlinear function $f(I)$ is Kerr-like at low I, but saturates for $I \gg 1/a$.

We then search for spherically symmetric solitary wave solutions to the GNLSE of the form $E(z, r = \sqrt{x^2 + y^2 + t^2}) = \exp(i\beta z)U(r)$, where β is a real propagation parameter that determines the bullet's radial profile. The real amplitude U is assumed to have its maximum value at $r = 0$, while $U_r, U_{rr} \to 0$ as $r \to \infty$. With this assumed form, Eq. (1) then reduces to the ordinary nonlinear differential equation

$$U_{rr} + \frac{2}{r}U_r + 2U[f(U^2) - \beta] = 0, \quad (2)$$

which can be numerically solved to yield radial solitary wave profiles. The inset of Fig. 1 shows such radial bullet profiles for $\beta = 3$, 6, and 12. Note that the pulses become taller and wider for increasing β. Calculating the bullet energy content $P = \int_0^\infty U^2 r^2 dr$ as a function of β yields the main figure with the three β values indicated. The corresponding energies are 1.28, 2.57, and 17.3, respectively. This distinctive U-shaped curve (the left negative-slope branch of the curve is barely visible due to the figure scale) is characteristic of saturable refractive index models (see, e.g, Ref. [11]) and not just the specific form chosen for this study. The minimum in the energy curve is $P_{\min} \simeq 0.97$ occurring for $\beta_{\min} \simeq 1$. For $P < P_{\min}$, spherical solitary waves are not possible, i.e., there exists an energy threshold for light bullet formation. One finds numerically that the solitary waves on the negative-slope branch ($\beta < \beta_{\min}$) of this curve are unstable to small perturbations, even numerical noise. Scattering simulations for this paper will be confined to the three bullet profiles shown which lie on the stable positive-slope branch of the U-shaped energy curve.

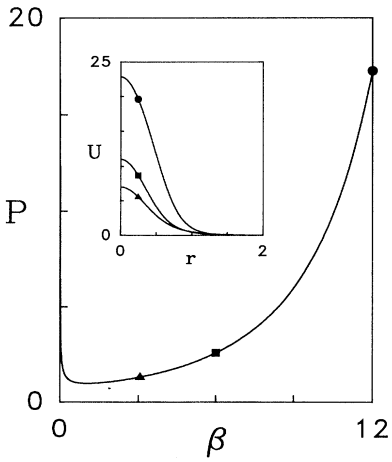

FIG. 1. Solitary wave energy versus β. Inset: radial solitary wave profiles $U(r)$ for $\beta = 3$ (triangle), $\beta = 6$ (square), and $\beta = 12$ (circle).

III. NUMERICAL METHOD

Most [12] scattering studies were carried out on a $128^2 \times 64$ rectangular mesh using the split-step Fourier method (SSFM) [13] to propagate the initial bullet configuration according to Eq. (1). The step size δz was typically taken to be 0.01, but was decreased to as low as 0.005 for $\beta = 12$ simulations in order to maintain numerical stability. The SSFM is a pseudospectral method accurate to second order in the step size. The method works as follows. The linear part of the partial differential equation is solved exactly in the Fourier domain for a half step $\delta z/2$ using the prescription

$$\tilde{E}\left(z + \frac{\delta z}{2}\right) = \exp\left(-i\frac{k^2}{2}\frac{\delta z}{2}\right)\tilde{E}(z), \quad (3)$$

where $\tilde{E}(z)$ is the Fourier transform of $E(z)$ and k is the magnitude of the wave vector in the Fourier domain. This portion of the scheme has the effect of spreading the pulse due to dispersion (diffraction) in the longitudinal (transverse) directions, respectively. The nonlinear part of the equation

$$iE_z + f(I=|E|^2)E = 0 \quad (4)$$

is then solved for another half step $\delta z/2$. In our case, this can be done exactly

$$E\left(z + \frac{\delta z}{2}\right) = \exp\left(if(I)\frac{\delta z}{2}\right) E(z). \quad (5)$$

The nonlinear part of the equation effectively serves to squeeze the pulse and counteract the effects of dispersion and diffraction. This cycle of linear followed by nonlinear advance constitutes an advance in "time" of δz and is remarkably fast compared to traditional explicit schemes due to the use of the fast Fourier transform with radix 2 mesh dimensions.

Numerical accuracy was checked by repeating the simulations with different mesh sizes and integration time steps δz, as well as monitoring various conserved quantities such as the total energy and the longitudinal and transverse momentum of the system.

Visualization of our three-dimensional data sets was achieved by producing color-coded $|E|$ animations of a

two-dimensional (2D) mesh slice. The asymptotic scattering angles for the 64 simulations that comprise our data were extracted from these 2D animations.

For a given scattering simulation there are a multitude of parameters to choose (Fig. 2). As mentioned previously, the propagation constant β determines the radial profile of the input bullets. The initial positions of the bullets with respect to the center of the computational mesh are given by the offset parameters $\pm t_0$ and $\pm x_0$. One can also introduce initial constant phase factors ϕ_1 and ϕ_2 by multiplying the individual input profiles by $\exp(i\phi_1)$ and $\exp(i\phi_2)$ for bullets 1 and 2, respectively. Finally, velocities $\pm v$ relative to the group velocity are introduced by taking input profiles of the form $U(r)\exp(\pm ivt)$. With ϕ the same for both pulses (i.e., $\phi_1 - \phi_2 = 0$), the bullets are attractive, bending towards each other as each bullet "sees" an increased refractive index due to the presence of the other bullet's "tail" [i.e., $U(r)$ at large r]. As already mentioned, this attractive force can result in spiraling behavior, eventually ending in light bullet fusion. For the scattering experiments reported here, we set $\phi_1 - \phi_2 = \pi$ so that the bullets are repulsive and symmetrically scatter from one another. As one moves away from $\phi_1 - \phi_2 = \pi$, the scattering becomes asymmetric with an energy exchange between solitons, the bullet leading in phase growing at the expense of the other [5].

Because the simulations are carried out in a box of finite size, the size being limited by the computer power used [14], several practical issues had to be dealt with in order to obtain accurate scattering data. Although the bullets tend to look like small billiard balls because of the rapid intensity drop-off with increasing r, nevertheless the tail of each bullet "sees" the tail of the other and one must check that the scattering results are independent of the initial separation t_0 (i.e., that initially the bullets are effectively infinitely separated). For example, Fig. 3 shows how the asymptotic scattering angle θ plateaus as t_0 is increased for two $\beta = 6$ light bullets initially incident with $v = 0.5$, impact parameter $b = 0.8$, and saturation parameter $a = 0.05$. (This a value was used for all simulations reported in this paper although, as we shall see, it plays no role in the light bullet interactions.)

Another concern is that if the impact parameter b becomes too large, the solitons will see each other across the periodic boundary and the scattering results will again be adversely affected. One must also be quite sure that the angle measured is in fact the asymptotic scattering angle θ. These and other issues connected to the finite size of the computational box have been carefully considered in presenting our final scattering data.

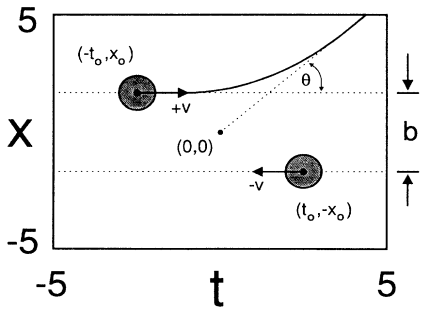

FIG. 2. Schematic representation of scattering experiments in the x-t plane. The rightmost bullet scatters symmetrically to the leftmost bullet.

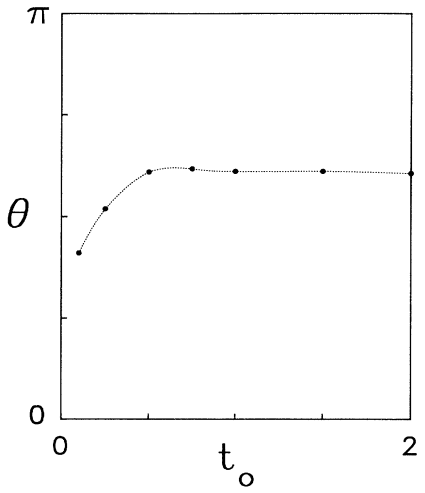

FIG. 3. Dependence of the asymptotic scattering angle θ on initial $\beta = 6$ bullet separation for $v = 0.5$, $b = 0.8$ collisions.

IV. RESULTS

A typical numerical scattering experiment is rendered in Fig. 4. Two $\beta = 6$ light bullets are initially positioned at $t_0 = \pm 2$ and $x_0 = \pm 0.4$ (corresponding to an impact parameter $b = 0.8$) with $v = 0.5$. As the simulation proceeds, the bullets approach and meet at $z = 3.0$, compressing slightly before scattering at an angle slightly greater than $\theta = \pi/2$. The particle or billiard-ball-like nature of the light bullets is quite evident. The light bullets are clearly not hard spheres as they compress slightly along their contact edge at $z = 3.0$. The force appears to be short ranged as the bullets rapidly regain their sphericity. Indeed they have done so by $z = 3.8$ (not shown). That the collision is almost completely elastic is confirmed by comparing the initial and final bullet profiles and energies. Figure 5 shows a least-squares fit to the leftmost light bullet at $z = 6.5$ in Fig. 4. The circled data values are numerical points taken from the computational mesh (for clarity we plot only 20% of the total points gathered) while the solid line is the best fit profile with $\beta = 5.9$. The upper and lower dashed curves are profiles for $\beta = 6.2$ and $\beta = 5.6$, respectively. The input profile of $\beta = 6.0$ (not shown) is so close to the experimental points that it is virtually indistinguishable from the solid curve. A very small amount (approximately 2%) of radiation has been shed which, because of its low intensity and the color cutoff, is not apparent in Fig. 4. In terms of the $P(\beta)$ curve in Fig. 1, the final state is still inside the square data point shown. For the simple saturable model, the light bullets are very stable against

large perturbations, undergoing nearly elastic collisions with each other.

We have performed a complete set of scattering studies for various impact parameters and speeds $v = 0.1$, 0.25, and 0.5, culminating in asymptotic scattering angle θ versus b curves for $\beta = 3$, 6, and 12 (Figs. 6–8). (The solid lines are theoretical fits to an elastic scattering model, which will be discussed in detail in Sec. V.) We see the expected behavior that $\theta \to \pi$ as $b \to 0$ with the bullets colliding head-on and reversing direction. In addition, $\theta \to 0$ for increasing b, the bullets passing by each other with decreasing interaction. Also, for a given b, the scattering angle is smaller for collisions at higher velocity as the bullets spend less time interacting with each other.

Before proceeding to the analysis, we should briefly estimate the error in our $\theta(b)$ measurements. As mentioned previously, the θ values are extracted from two-dimensional 128×128 pixel animations corresponding to a slice through our 3D mesh in the x-t plane. One calculates θ by forming a triangle whose hypotenuse is tangent to the asymptotic trajectory. Assuming a single pixel error in locating the end point of the hypotenuse, one can determine $d\theta/\theta \sim 3\%$ as representative of the error associated with this procedure. The error in θ due to the step size δz, initial t_0 separation, and across-boundary effects are believed to be negligible. The numerical (i.e., algorithmic) error due to the coarseness of our grid could be ascertained by performing simulations on much finer meshes, which is beyond our current computational power.

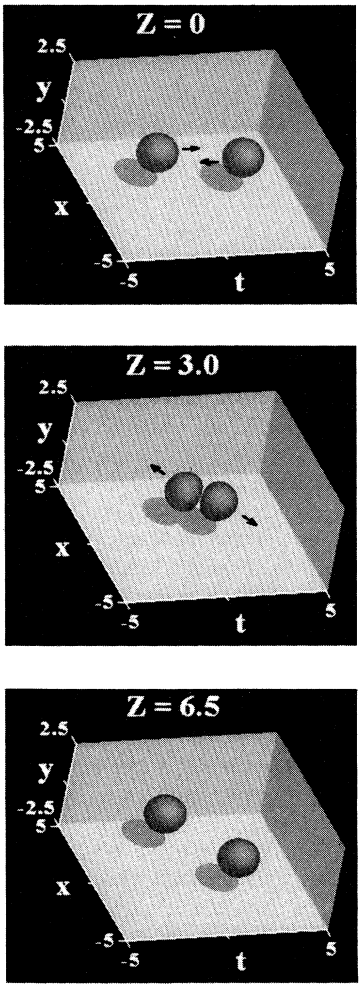

FIG. 4. Typical scattering simulation for two $\beta = 6$ light bullets incident at $v = 0.5$ and $b = 0.8$.

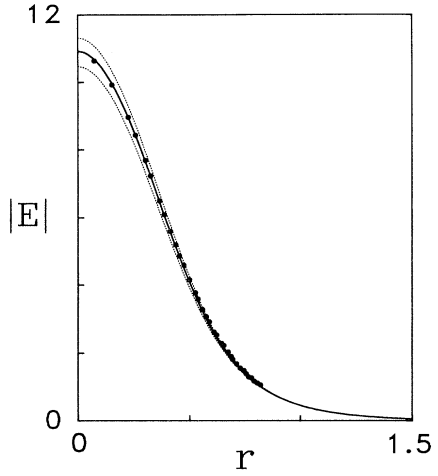

FIG. 5. $\beta = 5.9$ fit at $z = 6.5$ of the initially leftmost $\beta = 6$ light bullet in Fig. 4.

V. ANALYSIS

To quantitatively analyze the scattering data, we assume that we have a particle incident at impact parameter b with initial kinetic energy T upon a central

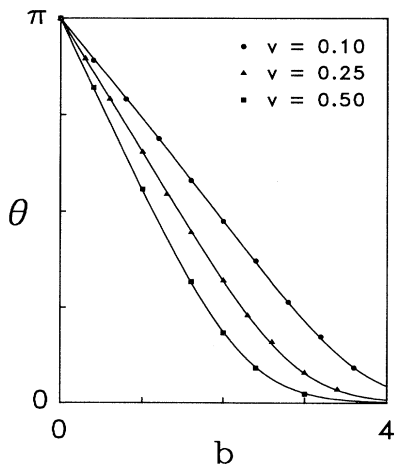

FIG. 6. Asymptotic scattering angle θ versus impact parameter b curves for scattering of two repulsive $\beta = 3$ light bullets at three collision velocities. The solid lines are theoretical fits.

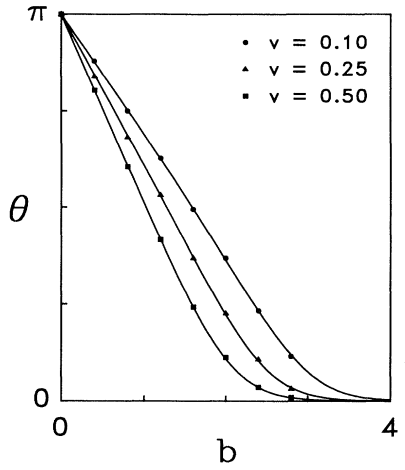

FIG. 7. θ versus b curves for $\beta = 6$ light bullets at three collision velocities. The solid lines are theoretical fits.

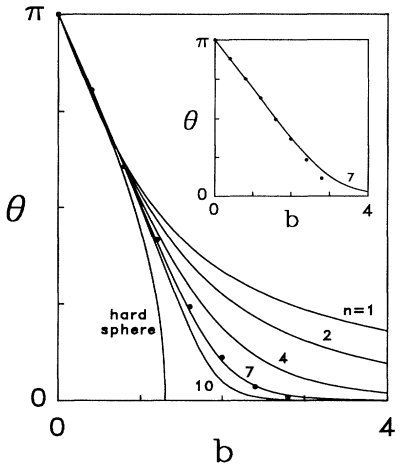

FIG. 9. Least-squares fit to $\beta = 6$, $v = 0.5$ scattering data for various polynomial models $V(r) \propto r^{-n}$ and a hard sphere model. Inset: optimum least-squares fit to $\beta = 6$, $v = 0.1$ scattering data for the $n = 7$ polynomial model.

force scattering potential $V(r)$. Our scattering problem is equivalent to this scenario for symmetric bullet collisions where θ is measured in the center of mass frame (as in Fig. 2 and all of our simulations). The asymptotic scattering angle θ can then be formally written [10] as

$$\theta = \pi - 2\int_{r_{\min}}^{\infty} \frac{(b/r^2)}{\sqrt{1-(b/r)^2 - V(r)/T}}\, dr, \qquad (6)$$

where r is the interparticle distance and $r_{\min}$ is the distance of closest approach. While this integral can be solved analytically for several low-order polynomial models $V(r)/T = Cr^{-n}$, e.g., the Coulomb potential with $n = 1$, it must generally be solved numerically.

Figure 9 shows least-squares fits of the low b, linear portion of the $\beta = 6$, $v = 0.5$ scattering data (bottommost points in Fig. 7) to various polynomial models for integer n. Also shown is the least-squares fit for a hard sphere model for which θ goes to zero at finite b, the impact parameter at which the light bullets pass at grazing incidence. From this figure it is clear that the potential is relatively short ranged, with the best fit occurring for $n \simeq 7$. However, as the inset shows, one cannot then fit the $\beta = 6$, $v = 0.1$ scattering data with the $n = 7$ polynomial model, the best fit occurring for $n = 10$ (not shown). This scenario holds for all of the scattering data, one finding that any two sets of curves at a given β value cannot be fitted by the same (even noninteger) n value. Since n (i.e., the structure of the force law) should remain fixed as v is varied, a polynomial model must be rejected.

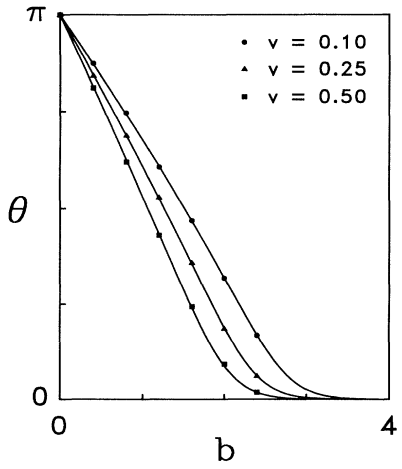

FIG. 8. θ versus b curves for $\beta = 12$ light bullets at three collision velocities. The solid lines are theoretical fits.

Having ruled out polynomial models, what should we take as an approximation to the correct interaction potential? Let us assume that the interaction is dominated by each bullet seeing the rapidly decreasing tail of the other. For the Kerr case in one dimension, the solitary wave behaves like $\exp(-\gamma r)$ for large r, with the decay constant $\gamma = \sqrt{2\beta}$. Coalescence between initially adjacent in-phase one-dimensional pulses is found to be exponential with this same decay constant [13]. Taking Eq. (2), which determines our light bullet radial profile, we assume that in the tail region $f(U^2) \ll \beta$, i.e., that for the saturable model, the intensity $I = U^2 \ll \beta/(1-a\beta)$. For $a = 0.05$, we need $U \ll 1.9$, 2.9, and 5.5 for $\beta = 3$, 6, and 12, respectively. Dropping the $f(U^2)$ term in Eq. (2), we obtain a modified Bessel equation, the relevant physical solution of which is $U(r) \propto \exp(-\gamma r)/r$. For $\beta = 3$, 6, and 12, $\gamma = 2.45$, 3.46, and 4.90, respectively.

In Eq. (6), we assume that $V(r)/T = C\exp(-\alpha r)/r$, i.e., of the form of a Yukawa potential. We shall determine α and C by least-squares fitting this model to our scattering data. If the tails of the bullets dominate the interaction, we would expect that $\alpha \simeq \gamma \equiv \sqrt{2\beta}$. Further, since $T \sim v^2$, we might expect that $\sqrt{C}$ scales as $1/v$.

Defining a least-squares merit function

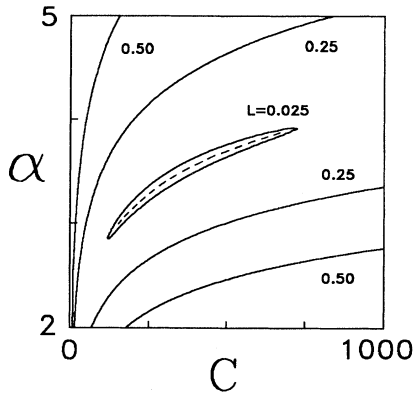

FIG. 10. Contours of constant merit function L in the α-C plane for $\beta = 6$, $v = 0.5$ scattering data and the Yukawa interaction potential $V(r)/T = C\exp(-\alpha r)/r$. The dashed line indicates the valley bottom.

$$L(\alpha, C) = \sqrt{\frac{1}{n}\sum_{i=1}^{n}[\theta_{\text{theory}}(\alpha, C; b_i) - \theta_{\text{num}}(b_i)]^2}, \quad (7)$$

which is positive definite and disappears for an exact fit between theory and numerical experiment, we search for α and C that minimize this function for a given set of $\theta(b)$ scattering data. Note that L corresponds to the mean vertical deviation between points on the numerical and theoretical scattering curves.

Figure 10 shows contours of constant L in the α-C plane for the $\beta = 6$, $v = 0.5$ scattering data. We see a long narrow valley for $L = 0.025$ and, as the minima must lie within this region, α is restricted to be between 3 and 4. Note that $L = 0.025$ indicates an extremely small mean deviation between theory and numerical experiment. If we traverse the valley from one end to the other, along the dashed line shown (which represents the floor of the valley), we obtain the $v = 0.5$ curve shown in Fig. 11, the minimum of which is at $\alpha = 3.32$. We then repeat this process for the $v = 0.1$ and $v = 0.25$ scattering data obtaining the other curves shown in Fig. 11 (each of which has a 2D merit function qualitatively similar to Fig. 10). The minima are at $\alpha = 3.30$ and 3.55 for $v = 0.1$ and 0.25, respectively. As for the polynomial model, we expect the decay constant α to be velocity independent and therefore take our optimal $\overline{\alpha}$ to be the mean value $\overline{\alpha} = 3.40$. This differs by only 2% from the "theoretical" value $\sqrt{2\beta} = 3.46$. That these L minima do not occur for exactly the same α value is due to a combination of numerical error, the error in extracting $\theta(b)$ from 2D animations, and slightly inelastic behavior.

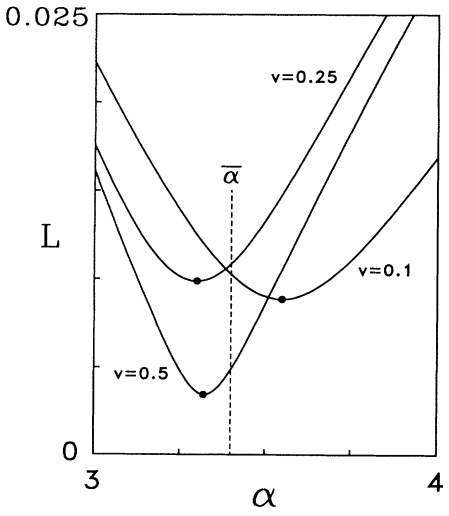

FIG. 11. $v = 0.5$ curve is a plot of L versus α along the dashed line shown in Fig. 10. $v = 0.25$ and $v = 0.5$ curves are similarly obtained from their respective scattering data. $\overline{\alpha}$ (vertical dashed line) is calculated as the mean value of the three minima shown.

TABLE I. Calculation of $\overline{\alpha}$ and a comparison with the "ideal" value $\sqrt{2\beta}$.

β	v	$\alpha_{\min}$	$\overline{\alpha}$	$\sqrt{2\beta}$
	0.1	2.41		
3	0.25	2.36	2.46	2.45
	0.5	2.60		
	0.1	3.55		
6	0.25	3.30	3.40	3.46
	0.5	3.32		
	0.1	4.79		
12	0.25	4.74	4.62	4.90
	0.5	4.32		

This procedure is repeated for the $\beta = 3$ and $\beta = 12$ sets of scattering curves yielding qualitatively similar results, which are summarized in Table I. Although there is a hint of a systematic trend in $\overline{\alpha}$ deviating from $\sqrt{2\beta}$ as β is increased, given the numerical uncertainty already discussed (on the order of several percent), it would be pushing our analysis too far to attempt to calculate next-order corrections to the Yukawa potential.

With the average least-squares $\overline{\alpha}$ values determined, we can then identify the corresponding C values for each velocity curve by reference to their respective L contour map (e.g., Fig. 10 for $\beta = 6$, $v = 0.5$). Both these C

TABLE II. C values and velocity scaling ratios.

β	v	$C_v(\overline{\alpha})$	$\sqrt{\frac{C_{0.1}}{C_{0.25}}}$	$\sqrt{\frac{C_{0.1}}{C_{0.5}}}$	$\sqrt{\frac{C_{0.25}}{C_{0.5}}}$
	0.1	3158			
3	0.25	476.6	2.57	5.13	1.99
	0.5	120.2			
	0.1	7245			
6	0.25	1265	2.39	4.91	2.05
	0.5	300.2			
	0.1	64 560			
12	0.25	10 450	2.49	5.23	2.11
	0.5	2356			
"Ideal" scaling[a]			2.50	5.00	2.00

[a]Ideal velocity scaling is $\sqrt{\frac{C_{v_1}}{C_{v_2}}} = \frac{v_2}{v_1}$.

TABLE III. Calculation of average Cv^2 values at a given β value.

β	v	Cv^2	$\overline{Cv^2}$
	0.1	31.58	
3	0.25	29.79	30.47
	0.5	30.05	
	0.1	72.45	
6	0.25	79.06	75.52
	0.5	75.05	
	0.1	645.6	
12	0.25	653.1	629.2
	0.5	589.0	

values and the calculated velocity scaling ratios are presented in Table II. These are the $\overline{\alpha}$ and C values used to produce the theoretical fits shown previously in Figs. 6–8. The theoretical curves fit the experimental data extremely well (as one expects with mean deviations on the order of 0.025). The scaling ratios shown in Table II are all within a few percent (maximum deviation of 5%) of the ideal values of 2.5, 5, and 2, further proof of the validity of our elastic scattering model and the choice of the Yukawa interaction potential.

We can look at our numerical data in still another way by appealing to a familiar example. For the (attractive) gravitational force problem involving two identical masses m and using the same initial conditions as in Fig. 2, we would have $V(r)/T = C/r$ with $C = Nm/v^2$, N being a numerical factor. Note that the product Cv^2 is (i) invariant for a given mass and (ii) increases linearly with mass.

For our light bullet problem, independent of any interpretation, we can also form the product Cv^2 for different v values as a function of β (Table III). The Cv^2 values are approximately constant for each β value, deviating with a small error consistent with our estimated numerical uncertainty from the average value $\overline{Cv^2}$. Analogous to the gravitational problem, $\overline{Cv^2}$ increases with increasing β or, from Fig. 1, with increasing bullet energy P. In Fig. 12, we have plotted $\overline{Cv^2}$ versus P, the experimental points being described by the linear equation $\overline{Cv^2} = 37.5P - 19.2$. The vertical cutoff (dashed line) corresponds to $P = P_{\min}$, the minimum energy required for bullet formation.

Comparing with conditions (i) and (ii) on $\overline{Cv^2}$ for the gravitational problem, we see that P appears to play the role of an effective mass with the caveat that there exists a minimum "mass" threshold for light bullet formation.

VI. CONCLUSION

We have numerically studied symmetric collisions between two identical light bullets differing in initial phase

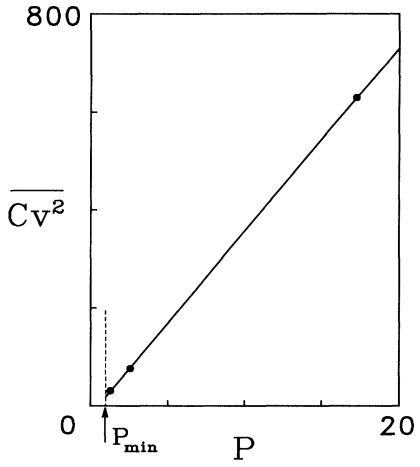

FIG. 12. $\overline{Cv^2}$ versus bullet energy content P.

by π radians for the saturable Kerr nonlinearity. On the positive slope of the bullet energy (P) vs phase shift parameter (β) curve, the light bullets were found to be stable against large perturbations (collisions) over a wide range of initial velocities and P values. The collisions were observed to be nearly elastic, the dynamics pictorially resembling that of two colliding billiard balls. By extracting the asymptotic scattering angle as a function of impact parameter, we were able to deduce that the repulsive interaction potential is short ranged and of the Yukawa form $\exp(-\alpha r)/r$, with the decay constant $\alpha \simeq \sqrt{2\beta}$. The form of the potential consistent with the scattering data follows from the governing equation when the intensity is sufficiently low that the nonlinearity can be neglected compared to β. Thus, in our collision experiments, each bullet saw only the tail of the other. Although the form of the nonlinearity plays an important role as far as stability is concerned, it proved to be unimportant in the bullet collisions. Based on the particle picture, we were able to account for how the scattering data scaled with velocity. Further, we showed that P plays the role of an effective mass above the energy threshold for bullet formation.

ACKNOWLEDGMENTS

The authors wish to thank the HPC High Performance Computing Centre for the opportunity to perform computational experiments on the Fujitsu VPX240/10. This research was supported by an operating grant from the Natural Sciences and Engineering Research Council of Canada.

[1] Y. Silberberg, Opt. Lett. **15**, 1282 (1990).
[2] R. H. Enns and S. S. Rangnekar, Phys. Rev. A **45**, 3354 (1992).
[3] R. H. Enns and D. E. Edmundson, Phys. Rev. A **47**, 4524 (1993).
[4] D. E. Edmundson and R. H. Enns, Opt. Lett. **17**, 586 (1992).
[5] D. E. Edmundson and R. H. Enns, Opt. Lett. **18**, 1609 (1993).
[6] N. Akhmediev and J. M. Soto-Crespo, Phys. Rev. A **47**, 1358 (1993).
[7] 3D animations of these and other simulations, viewable on DOS, Unix (X-Windows), and Macintosh systems, can be obtained by anonymous ftp from ftpserver.sfu.ca in the /pub/LightBullets directory.
[8] J. P. Gordon, Opt. Lett. **8**, 596 (1983).
[9] G. I. Stegeman and R. H. Stolen, J. Opt. Soc. Am. B **6**, 652 (1989).
[10] L. D. Landau and E. M. Lifshitz, *Mechanics*, 3rd ed. (Pergamon, Oxford, 1976).
[11] R. H. Enns, D. E. Edmundson, S. S. Rangnekar, and A. E. Kaplan, Opt. Quantum Electron. **24**, S1295 (1992).
[12] Some large impact parameter (small deflection) simulations were performed on an extended $256\times 128\times 64$ mesh to obtain more accurate asymptotic scattering angles.
[13] G. P. Agrawal, *Nonlinear Fiber Optics* (Academic, San Diego, 1989).
[14] Computationally our study represents 40 CPU weeks on an IBM RS/6000. For this reason a large portion of the simulations were performed on a 2.5 GFlop (peak speed) Fujitsu VPX240/10 supercomputer.

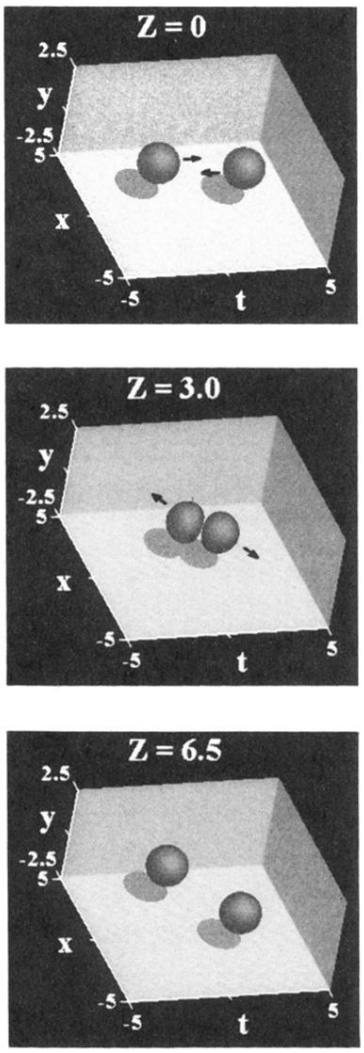

FIG. 4. Typical scattering simulation for two $\beta = 6$ light bullets incident at $v = 0.5$ and $b = 0.8$.